

Modeling of glow discharge-induced fluid dynamics

W. Shyy,^{a)} B. Jayaraman, and A. Andersson^{b)}

Department of Mechanical and Aerospace Engineering, University of Florida, Gainesville, Florida 32611

(Received 2 January 2002; accepted 23 August 2002)

Modeling of fluid dynamics and the associated heat transfer induced by plasma between two parallel electrodes is investigated. In particular, we consider a capacitively coupled radio frequency discharge plasma generator, where the plasma is generated on the surface of a dielectric circuit board with electrode strips on the top and bottom. The electrodes have a thickness of $100\ \mu\text{m}$, which is comparable to the height of the boundary layer. The regime considered is that the electron component is in the non-equilibrium state, and the plasma is nonthermal. Overall, due to the ion and large fluid particle interaction, the pressure is higher in the downstream of the electrode, causing the velocity structure to resemble that of a wall jet. Parameters related to the electrode operation, including the voltage, frequency, and free stream speed are varied to investigate the characteristics of the plasma-induced flow. Consistent with the experimental observation, the model shows a clear dependence of the induced jet velocity on the applied voltage and frequency. The heat flux exhibited a similar dependence on the strength of the plasma. The present plasma-induced flow concept can be useful for thermal management and active flow control. © 2002 American Institute of Physics. [DOI: 10.1063/1.1515103]

I. INTRODUCTION

Recent experiments conducted by Corke *et al.*¹ and by Roth *et al.*² have shown that interesting fluid flows can be induced by glow discharges. The device used in the experiments is a capacitively coupled radio frequency discharge plasma generator, placed on the surface of a dielectric circuit board with the electrode strips on the top and bottom. Figure 1 illustrates a staggered asymmetric configuration.

The plasma created by the device used by Roth *et al.*^{2,3} and by Corke *et al.*¹ is weakly ionized, low temperature (about room temperature) and nonthermal. This device contains no moving mechanical parts, and can be attractive for various applications, such as surface cooling, thermal management of electronic devices, and flow control. This type of plasma, formed between two parallel-plate electrodes, has been studied by Massines *et al.*,⁴ with additional background information offered in Refs. 5–7. In particular, Roth⁷ presents an analytical expression for the maximum induced velocity by treating the paraelectric force as an electrostatic pressure induced by the electric field gradients. In the analysis, the detailed balances between momentum transfer mechanisms, such as convection, hydrostatic pressure, viscous stresses, and electric field are not accounted for.

In the present study, a computational framework based on a phenomenological electromagnetic model, in conjunction with the Navier–Stokes equations, is developed to investigate the fluid flow and heat transfer resulting from glow discharges. The paraelectric force is modeled as a body force field over the region of plasma operation. In the following, we first offer an overview of the physical concepts and develop a computational capability for fluid flow and heat transfer resulting from the glow discharge. Next, we present

numerical results to highlight the solutions under several representative conditions.

II. PLASMA OPERATION AND FLUID FLOW

A. Non-equilibrium and Nonthermal Plasma

The plasma state is a result of adding sufficient amounts of energy to a molecular gas. The added energy causes the gas to dissociate as a result of collisions between those particles whose thermal kinetic energy exceeds the molecular

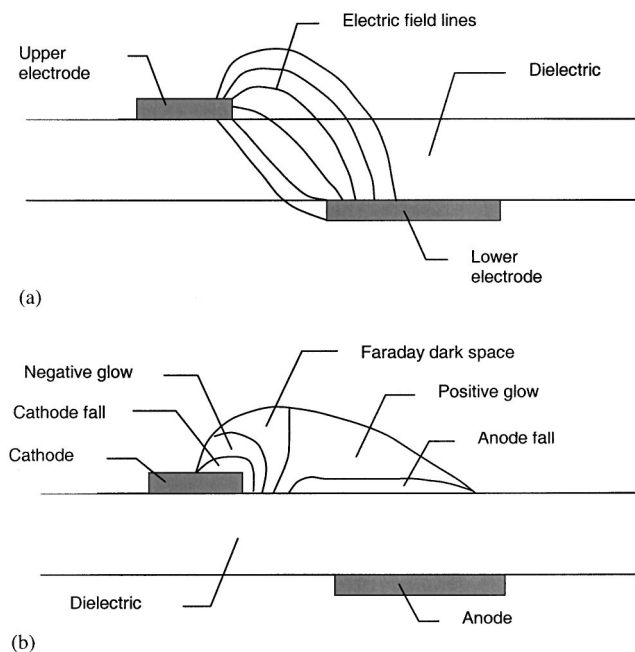


FIG. 1. Schematic representation of electrode geometry along with the field lines and the various glows associated with it during plasma formation. Note the concentration of field lines at the upper electrode and an even distribution on the dielectric.

^{a)}Electronic mail: wei-shyy@ufl.edu

^{b)}Also at: Department of Aeronautics, Aerodynamics Division, Royal Institute of Technology (KTH), 100 44 Stockholm, Sweden.

binding energy. As stated by Hippler *et al.*,⁵ the plasma is defined as a quasineutral particle system in the form of gaseous or fluidlike mixtures of free electrons and ions, frequently also containing neutral particles. Based on the extent of ionization, one observes either a fully ionized or a weakly ionized plasma. Weakly ionized plasma consists partly of ions and electrons and partly of neutral gas particles, i. e., atoms and molecules. Our interest is in weakly ionized gases.

The second classification based on temperature yields high- and low-temperature plasmas. Low-temperature plasmas can be classified as (i) only the electrons have a large mean kinetic energy, i. e., nonthermal plasma, and (ii) all components have a large kinetic energy compared to the neutral gas, i. e., thermal plasma. High-temperature plasmas are characterized by kinetic electron temperature of $T_e \approx T \geq 10^7$ K. Low-temperature thermal plasmas are characterized by a value of $T_e \approx T \leq 2 \times 10^4$ K. Finally, low-temperature nonthermal plasmas are characterized by temperature of $T \approx 300$ K and $T_e \leq 10^5$ K (Ref. 5). Here, T_e is the kinetic temperature of the electron component and T , the overall kinetic temperature.

The electric field acting on the charged particles, and especially on the electrons, is the main power source for the plasma considered. Owing to the small mass of the electrons, only a poor momentum transfer of the electrons with the heavy neutral particles of the plasma is realized by elastic collisions. Consequently, the electrons reach mean kinetic energy levels much higher than those of the neutral and charged heavy components, and the plasma becomes nonthermal. A significant portion of the electrons is energetically capable of overcoming the threshold above which inelastic electron collision processes take place. However, in each of these inelastic collision processes, the corresponding electron loses at least the threshold energy for the process, and the electron is transferred from a region of high kinetic energies to a low-energy region. Thus, the occurrence of inelastic collisions causes an efficient reduction of the electron energy. Consequently, the electron population in the region of inelastic collisions decreases markedly with increasing energy. This interplay between the action of the electric field and the elastic and inelastic collision processes causes the electron component to reach a state far from thermodynamic equilibrium.⁵

B. Plasma generation in an asymmetric plate configuration

Plasma operation between parallel plates has been extensively dealt with in literature. In the present study, we consider the plasma at atmospheric pressure generated by a radio frequency ac voltage. Massines *et al.*⁴ illustrate some of the physical features in such conditions for parallel plates. Many characteristics of plasma generation between parallel plates can be extended to the asymmetric configuration. The voltage and frequency used is of the order of a few kilovolts and few kilohertz, respectively. At such high frequencies, the charged particles (mainly electrons) attain high velocities. Also, these high frequencies leave a very short time for recombination. The ions, being the less mobile of the charged species, have no time to reach the electrode surface. This ion

trapping sustains the discharge by ensuring an adequate number of seed electrons at the beginning of each cycle. The discharge current is characterized by one peak per half cycle where the amplitude of the peak is of the order of milliamperes and the rise time is of the order of microseconds.⁴ There is also a small residual current between the discharges caused by the recombination of the charges. Hence, a main characteristic of this plasma is the periodicity of the current and the residual current, although this is limited by the frequency used (the periodicity is lost at frequencies 1 kHz or lower).⁴ The characteristic glows of such plasma are similar to those obtained for a dc case.

The plasma generation in an asymmetric electrode configuration is similar to that of the parallel-plate case; however, the presence of a dielectric separating the electrodes and the asymmetry lead to a qualitatively different pattern of electric field lines. The difference here is the curved field lines caused by the dominant fringe effects. In contrast to the parallel-plate case, the equipotentials in this configuration are not parallel. The asymmetric geometry with the lower electrode downstream and the associated glow regions are shown in Fig. 1.

The electric field distribution is strongest in the region closest to the inner edges of the two electrodes. This strength decreases in magnitude as one moves away from this region. It is easy to see that the probability for plasma formation is more in the region of stronger electric fields. When the voltage rises, the electrons leave the negative electrode (cathode and upper electrode for this half cycle) surface and move toward the anode. These electrons are involved in collisions with the neutral particles and ions causing further ionization. It should be noted that the anode surface here is not the electrode but the dielectric, which represents a pseudoanode. Restricted to a two-dimensional model, the surface area of the pseudoanode (in contact with the plasma) is much larger than that of the cathode in its vicinity. The anode fall immediately next to the pseudoanode is a region rich in electrons. One expects the distribution of charges on the surface of the dielectric to be similar to that of the cathode so that the distance between them is minimum. But this is not the case as the dielectric prevents the movement of charges on its surface in contrast to that of the cathode. Thus, we have a concentration of charges on the cathode and a comparatively sparse distribution of electrons on the pseudoanode. This leads to non-uniform field strength along the flow direction.

Even before the voltage reversal, the large memory voltage built up due to the charge separation aids recombination, which is seen as residual current. Our view is that the weaker electric field near the pseudocathode (the pseudoanode during the previous half cycle) renders the initial accelerating force aiding the recombination small when compared to the corresponding force during the previous half cycle. This, in turn, results in a lower energy level in the region of the plasma when compared to the previous half cycle. These electrons possess energy comparable to the threshold energy (for ionization) only as they reach the anode. During the recombination, the electrons reduce in number, especially so with no electron emission from the pseudocathode (as it is a dielectric). Thus, we have depopulation of the electrons due

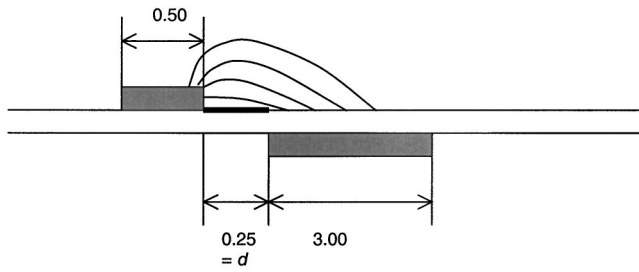


FIG. 2. Rough shape of electric field lines. The region with the strongest electric field, E_0 , is filled with black on the dielectric surface.

to recombination. The plasma formation during this half cycle depends on the presence of a critical number of electrons with the threshold energy. At lower frequencies, the recombination is high, and, hence there is very little or no plasma formation. In any case, we have only an insignificant plasma formation during this cycle. The ions accelerated during this non-uniform plasma generation can impart momentum to the fluid particles, resulting in an induced flow.

The non-uniform plasma generation explains the presence of the thrust in one direction alone. It should be stressed that while the electrons are of much higher velocity than ions, due to their small mass, their direct impact on momentum transfer is very small. Instead, between the plasma and ambient fluid, momentum transfer is realized via ions. In the present modeling framework, we will use the electric field as the key indicator to represent the paraelectric force and subsequently induced fluid flows. Roth⁷ explains the paraelectric force in terms of an electrostatic pressure exerted by the field lines, which tend to contract. This pressure, in turn, drives the fluid toward increasing electric field gradients. In this effort, we have incorporated the geometric effect of the electrodes and the resulting impact on the paraelectric force into the present computational model, as will be explained next.

III. DEVELOPMENT OF COMPUTATIONAL MODEL

Based on the aforementioned discussion, the combined effects of dielectric properties, electrode geometry, and operating frequency can induce fluid flow with potential for developing useful active control strategies and accelerate the convective heat transfer. In order to illustrate the induced fluid flow and model the heat transfer, a single pair of electrodes operating on the surface of a flat plate is considered. The asymmetric geometry used is the same as in Fig. 2. In order to predict the plasma induced flow, a quantitative model is presented next.

A. Body force formulation

The objective of the following formulation is to develop modeling concepts to account for the body force term acted by the plasma and on the fluid. As schematically illustrated in Fig. 2, the electric field lines are concentrated at the cathode and are almost uniformly distributed on the anode. It is reasonable to simply represent the field lines as parallel in most of the region except near the cathode. Thus, as schematically illustrated in Fig. 3, we can linearize the field

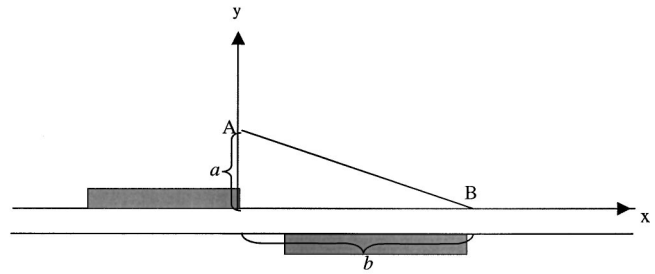


FIG. 3. The line A–B constitutes the plasma boundary using linear approximation. The electric field strength outside this line is not strong enough to ionize the air.

variation in space without computing the detailed electric field.

Specifically, the field lines here are such that the strength of the field decreases as one moves far away from the source. This variation of E the field strength, can be written as

$$|E| = E_0 - k_1x - k_2y, \quad (1)$$

where E_0 is the electric field in the darkened region in the Fig. 2. E_0 can be approximated as

$$E_0 = \frac{V}{d}, \quad (2)$$

where d is the separation between the two electrodes in the x direction. The constants are evaluated by using the condition that the field strength is the breakdown value at the plasma–fluid boundary. Hence, we can find k_1 and k_2 . The components of the electric field are given by

$$E_x = \frac{Ek_2}{\sqrt{k_1^2 + k_2^2}}, \quad E_y = \frac{Ek_1}{\sqrt{k_1^2 + k_2^2}}. \quad (3)$$

The period of interest during a particular cycle is the small time Δt during which the plasma discharge takes place. In the present asymmetric electrode, we have the high discharge currents and the resulting momentum transfer during a portion of the ac cycle. The magnitude of this Δt is small compared to the fluid time scales, especially so for the frequency range we are dealing with. Thus, the body force components along the x and y direction, f_x and f_y , are calculated as

$$f_x = E_x \rho_c e_c, \quad f_y = E_y \rho_c e_c. \quad (4)$$

This force acts only in the regions where the plasma is present which is determined by the field strength at the point. The delta function ensures this restriction, written as

$$\delta = 1 \quad \text{for } E < E_{cr}, \\ \delta = 0 \quad \text{for } E \geq E_{cr}.$$

The E_{cr} in this case is the breakdown electric field strength, E_b . The effective force on the neutral molecules is given by

$$f_{\text{eff}x} = \alpha f_x \delta, \quad f_{\text{eff}y} = \alpha f_y \delta, \quad (5)$$

where α is a factor to account for the collision efficiency. This force acts only during the time Δt (during which the plasma is formed), which corresponds to one half cycle, as already discussed. The force during the second half of the cycle can be neglected as it has little or no plasma formation. The high frequency of the discharge (around 5 kHz) makes it reasonable to consider the force acting on the fluid as a constant. Hence, the force can be time averaged over a complete cycle although it exists only for a small time Δt per cycle

$$F_{\text{tave}x} = \frac{f_{\text{eff}x} \Delta t}{T_t},$$

$$F_{\text{tave}y} = \frac{f_{\text{eff}y} \Delta t}{T_t}. \tag{6}$$

This time period of the cycle T_t is then period of the applied voltage. The time-averaged force can be written as

$$F_{\text{tave}x} = \vartheta f_{\text{eff}x} \Delta t,$$

$$F_{\text{tave}y} = \vartheta f_{\text{eff}y} \Delta t, \tag{7}$$

where ϑ (reciprocal of the time period) is the frequency of the applied voltage. These are represented as the body force components in the Navier–Stokes equations. In the present model, no attempt is made to establish a criterion for the plasma to be capable of inducing the fluid flow. Such a criterion requires a more detailed analysis of the plasma dynamics.

B. Governing equations

The numerical model consists of the continuity equation, the two-dimensional Navier–Stokes equations and the energy transport equation for a steady incompressible flow. The body force terms, which are added to the momentum equations, carry the effect of the plasma discharge on the fluid flow. The fluid is assumed to be incompressible in view of the plasma induced jet being a low Reynolds number and essentially isothermal phenomenon. The electric field along the straight line (Figs. 2 and 3) from (0,0) to (d , 0) is E_0 and hence $f=f_0$. Similarly, the electric field on the straight line joining (0, a) and (b , 0) has a value E_1 and hence $f=f_1$ all along its length. In the following, we offer a complete set of governing equations, in the two-dimensional form

$$\frac{\partial A}{\partial t} + \frac{\partial B}{\partial x} + \frac{\partial C}{\partial y} = D, \tag{8}$$

$$A = \begin{bmatrix} \rho \\ \rho u \\ \rho v \\ e \end{bmatrix}, \tag{9}$$

$$B = \begin{bmatrix} \rho u \\ \rho u^2 + p - \tau_{xx} \\ \rho u v - \tau_{xy} \\ u(e+p) - \tau_{xx}u - \tau_{xy}v - k \partial_x T \end{bmatrix}, \tag{10}$$

$$C = \begin{bmatrix} \rho v \\ \rho u v - \tau_{xy} \\ \rho v^2 + p - \tau_{yy} \\ u(e+p) - \tau_{xy}u - \tau_{yy}v - k \partial_y T \end{bmatrix}, \tag{11}$$

$$D = \begin{bmatrix} 0 \\ F_{\text{tave}x} \\ F_{\text{tave}y} \\ 0 \end{bmatrix}, \tag{12}$$

where τ_{xy} is the shear stress. The $F_{\text{tave}x}$ and $F_{\text{tave}y}$, body force terms given from Eq. (7) have a value of zero in a region where we do not have the plasma and take the following form under the influence of the plasma

$$F_{\text{tave}e} = \vartheta \alpha \rho_c e_c \Delta t E \delta, \tag{13}$$

$$\bar{E} = \left(\frac{E \cdot k_2}{\sqrt{k_1^2 + k_2^2}}, \frac{E \cdot k_1}{\sqrt{k_1^2 + k_2^2}} \right). \tag{14}$$

Boundary conditions

The no-slip condition when applied at the solid wall yields,

$$u = v = 0 \quad \text{at } y = 0. \tag{15}$$

At the outlets, zero-velocity gradient is assigned taking advantage of the negligible influence of the plasma, far downstream of the electrode. The plasma discharge boundary is specified by

$$\rho_c = 0 \quad \text{for } E < E_b. \tag{16}$$

C. Problem description

In order to simulate the experimentally observed flow effects, we compute the effect of our body force model on the flow over a small flat plate with the plasma generation device (upper electrode) attached to it. We will only focus on the vicinity of the electrode to investigate the detailed flow field. The flat plate is 20.5 mm long, with the upper electrode fitted 12 mm from the leading edge of the plate. The electrode has the length 0.5 mm and the height 0.1 mm. The height of the domain is 10 mm. The flat plate constitutes the lower boundary of the computational domain, with its leading edge 1 mm from the left boundary of the grid. Three grid blocks constitute the computational grid. The total number of computational meshes employed is 290×100. The chosen mesh distribution is clustered to focus the computational effort on the flow phenomena occurring around and after the upper electrode where the body force is applied. Figure 4 represents a schematic diagram of the computational domain. This grid size and distribution can produce satisfactory solutions in the present study.

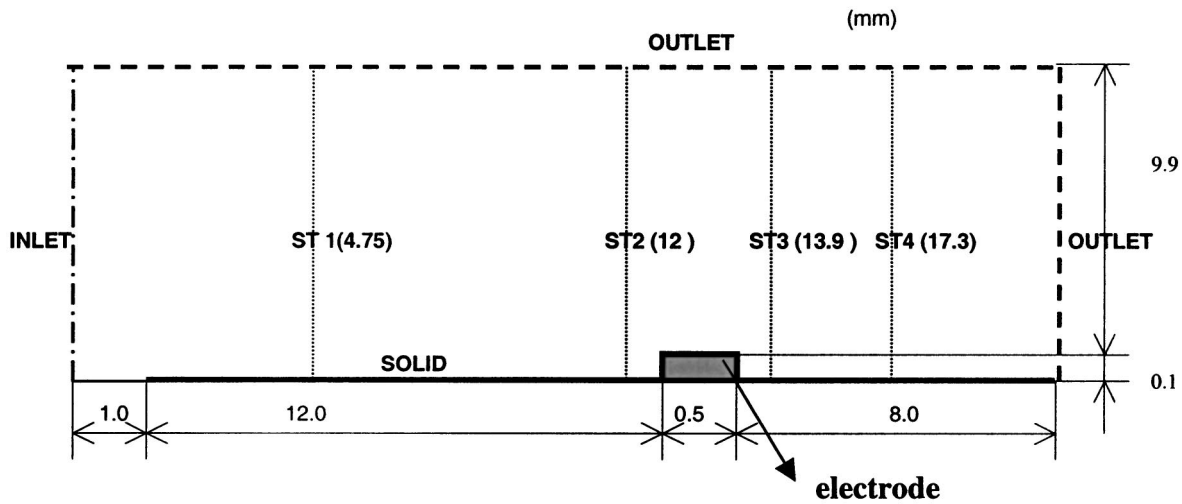


FIG. 4. The computational domain used for calculations shows the flat plate with the upper electrode. The various dimensions, the boundary specifications, and the stations are indicated with the coordinate of the plane in the parentheses.

The key dimensionless parameters in the present model are (i) Reynolds number,

$$\frac{\rho_m V_m L_m}{\mu_m} \tag{17}$$

(ii) The ratio of the body force to the inertial force,

$$\frac{\mu_m V_m L_m}{F_m} = \frac{\mu_e V_e L_e}{F_e} \tag{18}$$

where L is the characteristic length, V is the free stream velocity, F is the body force, ρ is the density, and μ is the coefficient of viscosity. The subscripts m and e represent the model and experimental values respectively.

For the numerical simulations, we used a pressure-based algorithm^{8,9} with a second-order upwind convection scheme.

IV. RESULTS AND DISCUSSIONS

In order to model the plasma effects as a body force, we use the same values of parameters as used in the experiments.^{2,3} Unlike in the experiments, the simulation is carried out for a single electrode panel. For the heat transfer computation, the surface in contact with the fluid has a temperature twice the ambient fluid temperature. All temperatures are nondimensionalized.

The various parameters required here are, ϑ is the frequency of applied voltage = 3 kHz, ρ_c is the charge density (electrons) = $1.0 \times 10^{11}/\text{cm}^3$, U_a is the applied voltage = 4 kV root mean square (rms), E_b is the breakdown electric field strength = 30 kV/cm,¹⁰ Δt is the discharge time = 67 μs , a is the height of the plasma = 1.5 mm, b is the width of the plasma = 3 mm (estimated from the picture in Ref. 2), and d is the distance between the plates = 0.25 mm.

The parameter k_1 is calculated from Eq. (1),

$$k_1 = \frac{E_0 - E_b}{b} = 6.54 \times 10^2 \text{ kV/cm}^2.$$

Similarly, $k_2 = 13.08 \times 10^2 \text{ kV/cm}^2$. E_0 , the maximum electric field in the plasma region can be calculated from Eq. (2) as

$$E_0 = \frac{U_0}{d} = 226.27 \text{ kV/cm}.$$

According to Eq. (1), the magnitude of E is

$$E(x, y) = |\mathbf{E}| = E_0 - k_1 x - k_2 y.$$

Equation (3) gives

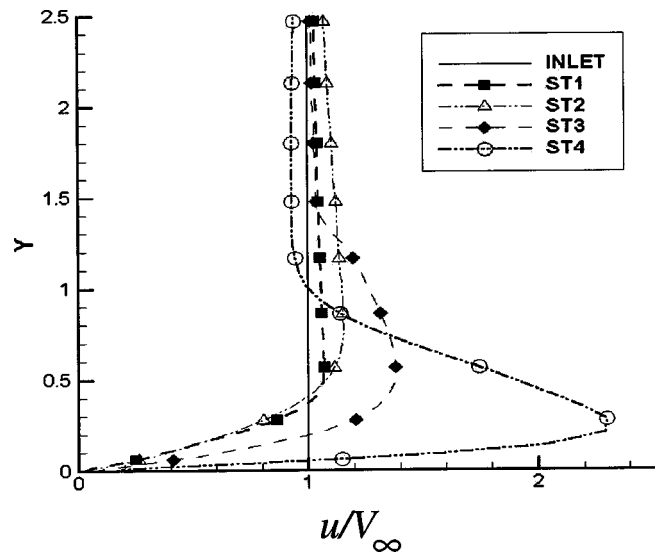
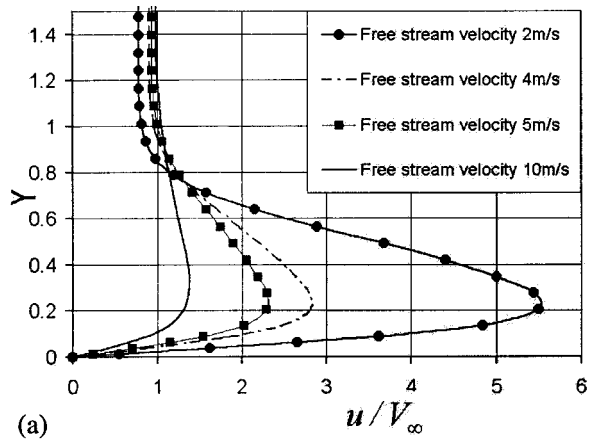
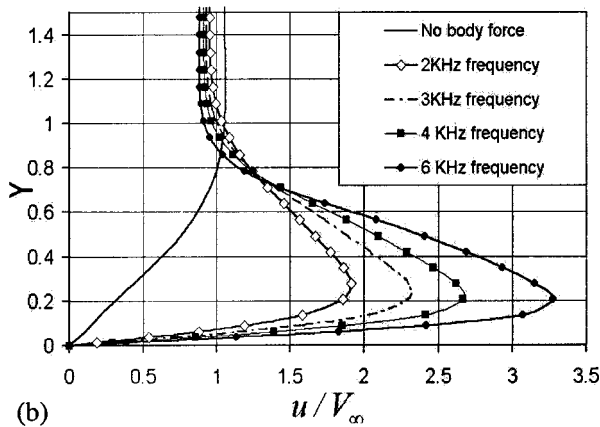


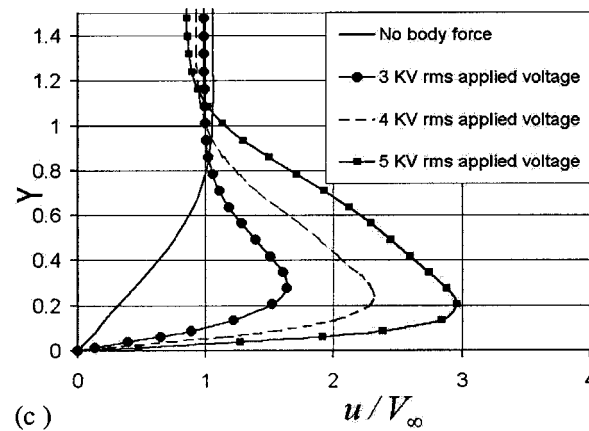
FIG. 5. The velocity profiles compared at the four different stations.



(a)



(b)



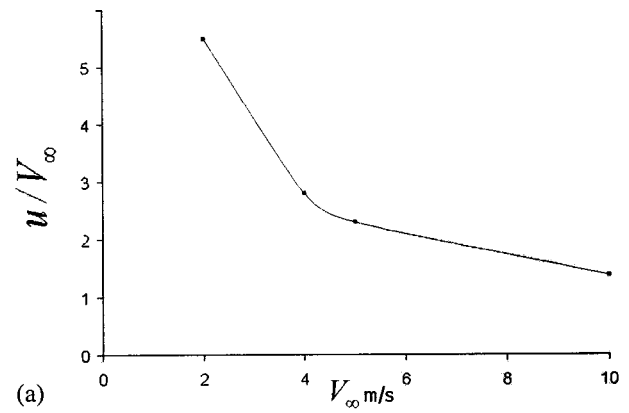
(c)

FIG. 6. Effect of the various parameters as seen from the velocity profiles. The comparison is done at ST4 (Fig. 4).

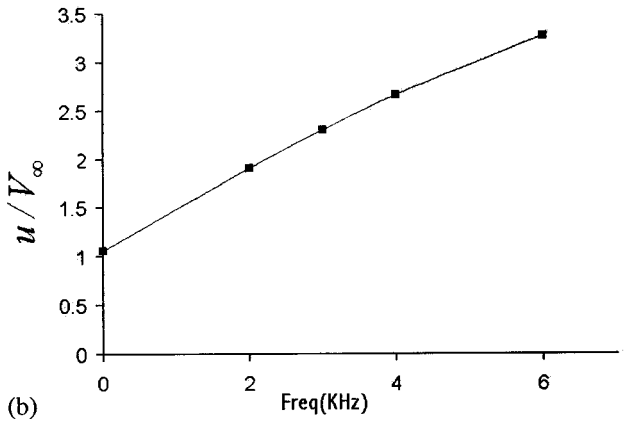
$$E_x(x, y) = \frac{E(x, y)k_2}{\sqrt{k_1^2 + k_2^2}} = 0.89 E,$$

$$E_y(x, y) = \frac{E(x, y)k_1}{\sqrt{k_1^2 + k_2^2}} = 0.45 E.$$

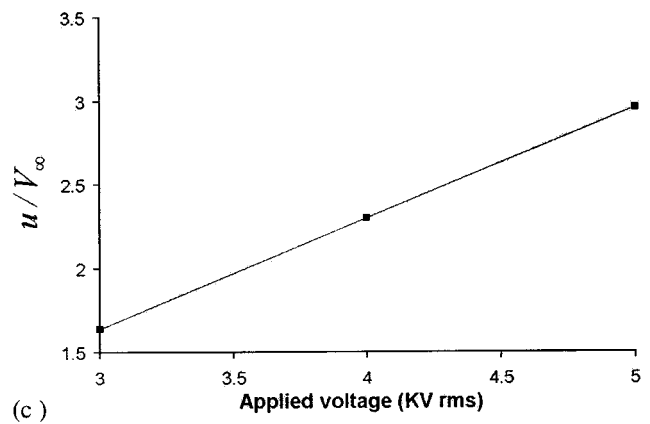
As mentioned earlier, ρ_c is a constant in the region of plasma formation and has a value of $10^{11}/\text{cm}^2$.^{2,3} Thus, the net force in the x and y directions can be calculated from Eqs. (4) – (7). The value of α can be assumed to be one in view of the disparity between the electron and neutral particle number densities. Thus, we get



(a)



(b)



(c)

FIG. 7. Effect of the various parameters on the peak velocity. All curves are plotted for ST4 (Fig. 4).

$$F_{\text{tave}x} = 2.88 \times 10^{-6} E,$$

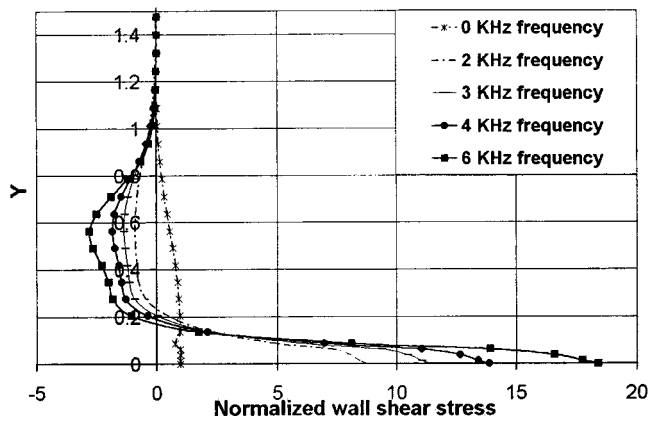
$$F_{\text{tave}y} = 1.44 \times 10^{-6} E,$$

where E has the unit of V/cm.

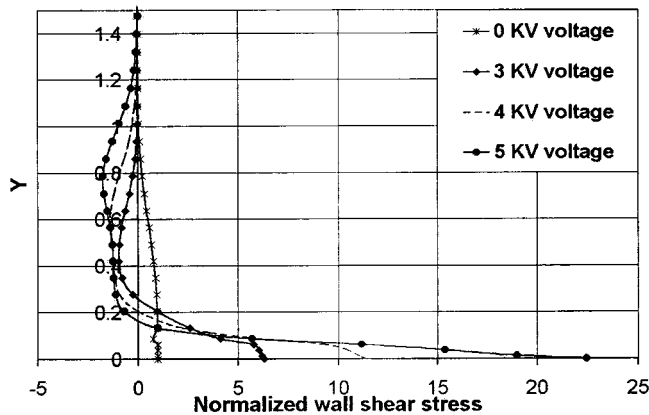
The values of the parameters for the different cases are listed below.

- (1) Free stream velocity, V_∞ : 2, 4, 5, and 10 m/s,
- (2) Applied voltage, U_a : 3, 4, and 5 kV rms, and
- (3) Applied frequency, ϑ : 2, 3, 4, and 6 kHz.

The corresponding Reynolds numbers based on these velocities and a characteristic length, $L_m = 0.1$ mm (the height of the electrode) are 13.7, 27.4, 34.2, and 68.5.

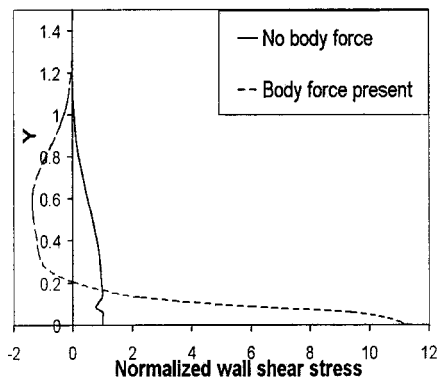


(a)

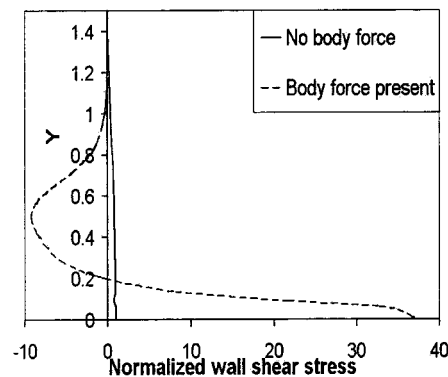


(b)

FIG. 8. Dependence of the wall shear stress on different parameters. All curves are plotted for ST4 (Fig. 4).



(c)



(d)

To study the variation of the velocity profile with the change in values of the key operating parameters (V_∞ , U_a , and ϑ), four different stations were chosen for the discussion whose positions are indicated in Fig. 4. The effect on the various regions of the fluid flow can be seen from the velocity profiles in Fig. 5. In accordance with expectations, the maximum peak value of the velocity is obtained downstream of the electrode (i. e., in the high-pressure region). The overshoot of the velocity above the free stream velocity gives the extent to which the plasma affects the flow. Overall, the velocity structure in the downstream of the electrode resembles that of a wall jet. With the mass being conserved at each vertical plane, the free stream velocity upstream of the electrode does not attain the far-field value, in trying to compen-

sate for the induced mass flux in the wall jet region. The free stream approaches the far-field value asymptotically as one moves far away from the electrode.

In the following studies, the parameters, which are maintained constant, are assumed the reference values of 4 kV, 3 kHz, and 5 m/s for the applied voltage, frequency, and velocity, respectively. Moreover, all the voltages used are rms values. In Fig. 6, a comparative study of the induced jet velocity profiles for the different operating parameters is presented. Figure 6(a) gives the normalized velocity profile at ST4 for the various free stream velocities. As expected, the plasma produces the maximum relative effect on the velocity profile for the case with the lowest value of the free stream velocity. Figures 6(b) and 6(c) give the normalized profiles

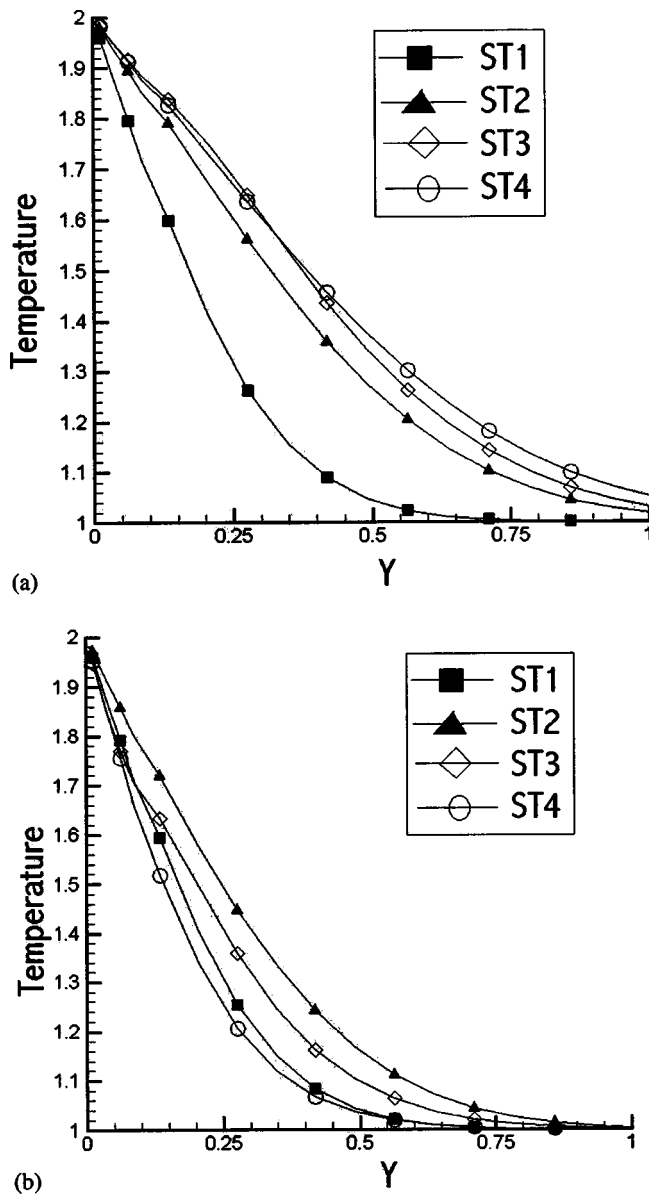


FIG. 9. The temperature profiles along the wall obtained in the presence (b) and absence (a) of plasma for $Re=34$ and $Pr=0.7$. See also Fig.4 for station details.

for the different applied voltages and frequencies. In both cases, the peak jet velocity increases with the electrode frequency and voltage, which can be attributed to the linear dependence of the body force on the applied voltage and frequency. It is worth mentioning that with the Δt being held constant, the frequency variation effectively presents a loading factor study. Figure 7(a) shows the peak-induced velocity variation with the free stream value. In Figs. 7(b) and 7(c), the peak jet velocity varies linearly with the applied voltage and frequency, respectively. Similar trends are also observed in the results presented by Roth.⁷ In fact, there is a reasonable agreement in magnitude for the peak velocities. The wall shear stress is also calculated for the cases mentioned herein. In Figs. 8(a) and 8(b), the wall shear stress is normalized with the corresponding peak value for the no-plasma case. In the presence of the plasma, the peak value of the wall shear stress is larger than that of the no-plasma case.

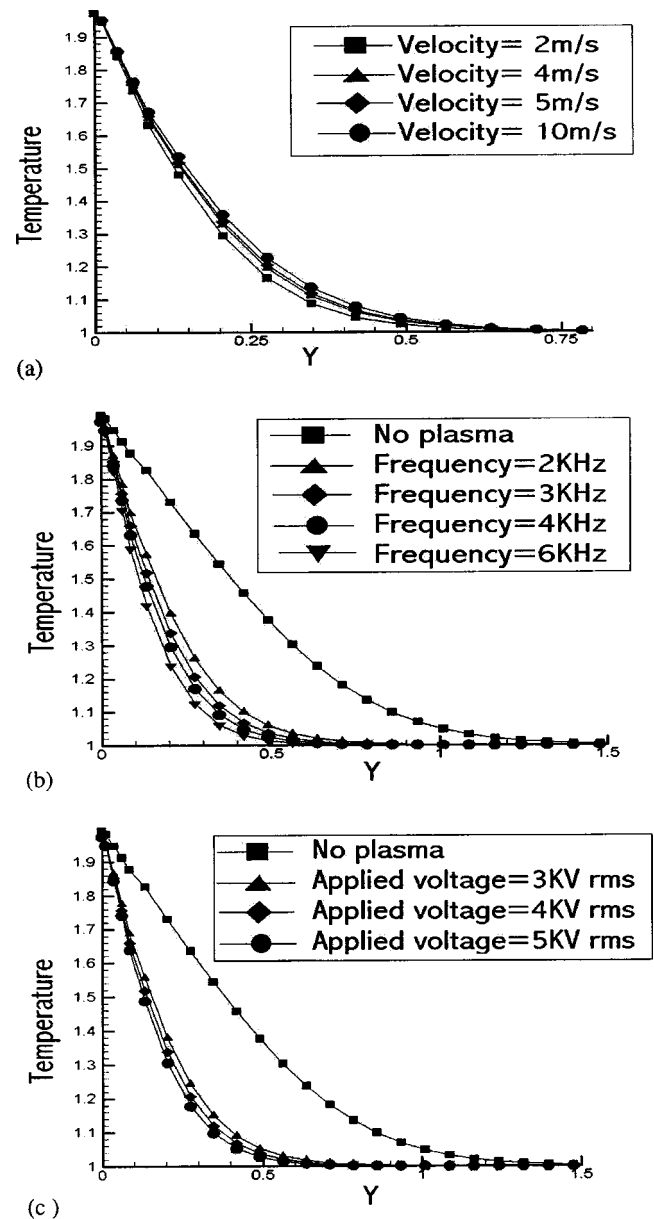


FIG. 10. Effect of the various parameters on the temperature profile at ST4 (Fig. 4).

Further away from the wall, the velocities reduce gradually to the free stream value, which explains the negative values taken by the shear stress. Figures 8(a) and 8(b) show the wall shear stress profiles for different frequencies and applied voltages, respectively. In Figs. 8(c) and 8(d), two flow fields with different free stream velocities (2 m/s and 5 m/s), but with similar plasma characteristics are compared. Here, the stress is normalized with the peak value obtained for the corresponding cases without plasma. The larger peak value obtained for the case with $V_\infty = 2$ m/s shows that the relative effect of the induced wall jet increases with decreasing free stream velocity.

In addition to the flow field, the effect of the induced jet on heat transfer from the surface has also been studied. Figure 9 presents the temperature profiles at the four stations. Figure 9(a) shows that the temperature gradient along the normal to the surface in ST2, ST3, and ST4 is smaller than

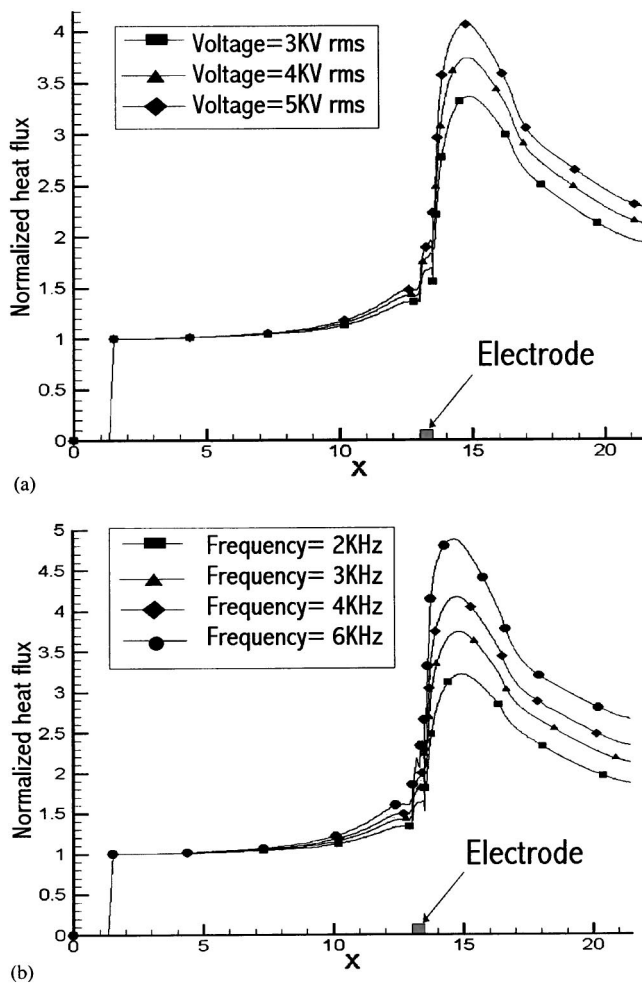


FIG. 11. Comparison of normalized heat flux for different voltages and frequencies. See also Fig. 4 for geometry details.

that at ST1. This is due to the viscous layer being thinner at ST1. The Reynolds number considered is 34 with a Prandtl number of 0.7. With the plasma operating, the temperature gradients increase in ST2, ST3 and ST4, but no appreciable change is seen in ST1. In Fig. 10, a parametric study for the temperature at ST4 is presented. Figure 10(a) presents the temperature profile for different free stream velocities. There is a perceptible effect on the profile with the higher velocity case having a larger temperature gradient. Figure 10(b) compares the no-plasma case and the cases with plasma of varying voltage and frequency. The voltage used here is 4 kV and free stream velocity is 5 m/s. There is a dramatic alteration of the profile caused by the plasma.

In Fig. 10(c), the temperature profile for plasma with different voltages is presented. The frequency used here is 3 kHz and the free stream velocity is 5 m/s. The thermal gradients here become higher for stronger plasma. Figure 11 presents the heat flux from the surface for different applied voltages and frequencies with a uniform inlet velocity of 5 m/s. In Fig. 11(a), the effect of the plasma is felt only from a small region upstream of the electrode which is the region containing ST2. All heat flux values were normalized using the corresponding no-plasma value. The maximum heat flux is about four times that for the no-plasma case for the

strengths of the plasma considered. This is at a point immediately downstream of the electrode. Further downstream, the effect of the plasma trails away. This pattern is seen for all the voltages considered and the magnitude of the flux out of the surface is proportional to the strength of the plasma. In Fig. 11(b), a similar comparison is shown for the different frequencies for an applied voltage of 4 kV. The heat flux pattern across the wall is similar to that obtained previously. The maximum heat flux in this case is around 4.5 times (with a frequency of 6 kHz) of that with no plasma. As expected, the peak flux varies proportionally with the applied frequency.

V. SUMMARY AND CONCLUSIONS

Motivated by the experimental studies by Roth *et al.*^{2,3,7} and Corke *et al.*,¹ a computational model for the glow discharge-induced fluid flow and heat transfer has been constructed. Basic features of the plasma physics along with an approximate modeling of the paraelectric effect on the flow are presented.

The paraelectric force can be realized by the dielectric characteristics, applied voltage, frequency, and the asymmetric configuration of the electrodes. Overall, due to the ions and neutral fluid particle interaction, the hydrostatic pressure is higher downstream of the electrode, causing a wall jet-type of flow to be induced. This plasma-induced jet can modify the surrounding flow structure and augment the heat transfer rate from the surface. The parameters related to the electrode operation, including the voltage, frequency, and free stream speed are varied to investigate the characteristics of the plasma-induced flow and the heat transfer characteristics. It is established that the induced flow velocities and heat flux vary proportionally with the applied frequency and voltage. In particular, the peak blowing velocity estimated by Roth⁷ is in agreement with the present effort. The findings are consistent with the experimental observations.^{2,3,7} Furthermore, the range of velocities for which the plasma is effective is also similar between our and previous studies. The maximum heat flux obtained from the parametric study is about 4.5 times that without plasma. Optimizing the electrode shape and operating conditions can further increase this value.

ACKNOWLEDGMENTS

The present research has been partially supported by the U. S. Air Force and TRW. The authors have benefited from the communication with Dr. Gregg Abate, Dr. John Anttonen, and Dr. Tom McLaughlin.

¹T.C. Corke, E.J. Jumper, M.L. Post, D. Orlov, and T.E. McLaughlin, Proceedings of the AIAA 40th Aerospace Sciences Meeting and Exhibit, 14–17 January 2002, Reno, NV.

²J.R. Roth, D.M. Sherman, and S.P. Wilkinson, Proceedings of the AIAA 36th Aerospace Sciences Meeting and Exhibit, 12–15 January 1998, Reno, NV.

³J.R. Roth, D.M. Sherman, and S.P. Wilkinson, AIAA J. **38**, 7 (2000).

⁴F. Massines, A. Rabehi, P. Decomps, R.B. Gadri, P. Ségur, and C. Mayoux, J. Appl. Phys. **83**, 6 (1998).

- ⁵ *Low Temperature Plasma Physics: Fundamental Aspects and Applications*, edited by S. Hippler, M. Pfau, K.H. Schmidt, and Schoenbach (Wiley-VCH, Berlin, 2001).
- ⁶ J.R. Roth, *Principles*, Vol. 1. Industrial Plasma Engineering (IOP, Bristol, 1995).
- ⁷ J.R. Roth, *Applications to Nonthermal Plasma Processing Industrial Plasma Engineering Vol. 2* (IOP Bristol, 2001).
- ⁸ W. Shyy, S. Thakur, H. Ouyang, J. Liu, and E. Blosch, *Computational Techniques for Complex Transport Phenomena* (Cambridge University Press, Cambridge, UK, 1997).
- ⁹ W. Shyy, *Computational Modeling for Fluid Flow and Interfacial Transport* (Elsevier, Amsterdam, 1994).
- ¹⁰ M. Capitelli, C.M. Ferreira, B.F. Gordiets, and A.I. Osipov, *Plasma Kinetics in Atmospheric Gases* (Springer, Berlin, 2000).